Catalysis Today 175 (2011) 216–222

Contents lists available at ScienceDirect

Catalysis Today

journal homepage: www.elsevier.com/locate/cattod

Catalytic combustion of methane over cerium-doped cobalt chromite catalysts

Jinghuan Chen [a], Wenbo Shi [a], Junhua Li [a,b,*]

[a] Department of Environmental Science and Engineering, Tsinghua University, Beijing, 100084, China
[b] State Key Joint Laboratory of Environment Simulation and Pollution Control (SKLESPC), Beijing, 100084, China

ARTICLE INFO

Article history:
Received 15 October 2010
Received in revised form 19 March 2011
Accepted 30 March 2011
Available online 5 May 2011

Keywords:
Methane combustion
Cobalt chromite
Cerium
Structure deformation

ABSTRACT

Cerium modified cobalt chromite catalysts were prepared via co-precipitation method and investigated for the catalytic combustion of methane. Characterization studies by X-ray diffraction (XRD), Raman spectroscopy, BET, scanning electron microscopy (SEM), X-ray photoelectron spectroscopy (XPS), temperature-programmed reduction mass spectroscopy (CH_4 TPR-MS) and temperature-programmed desorption of oxygen (O_2-TPD) were carried out.

An improvement of the catalytic activity was observed over cerium-substituted cobalt chromite catalysts with appropriate cerium substitution degrees. The best result has been attained with 5% cerium modified catalyst, for which 5% chromium in $CoCr_2O_4$ was substituted by cerium, and the catalytic activity reached 90% of methane conversion at 465 °C. The characterization results indicated that cerium doping could deform the spinel structure and cause redistribution of metal ions with different oxidation states; consequently, they would increase crystal defects and oxygen vacancy concentration, which facilitate oxygen mobility and thus increase the catalytic performance of cerium modified cobalt chromite catalysts.

1. Introduction

With the soaring gasoline prices and the increasingly strict emission limits, natural gas engines are widely applied to vehicles nowadays [1]. In addition to economic and political reasons, the use of compressed natural gas (CNG) for automotive applications offers significant environmental advantages over gasoline and diesel. However, the natural gas vehicles (NGVs) advantages are partially balanced by the emission of unburned methane. As one of greenhouse gases, methane is recognized to contribute more to global atmosphere warming than CO_2 at equivalent emission rates, all the more since its lifetime is quite long [1,2]. Therefore, the abatement of unconverted methane exhausted from CNG vehicles becomes rather important [3].

Catalytic combustion of methane is a promising technology that can convert methane into carbon dioxide at relatively low temperature, and is extensively studied over the last decade. Noble metal-based catalysts, especially Pd-based ones can exhibit outstanding catalytic behavior at low temperatures [3–6]. Nevertheless, catalysts based on transition metal oxides, such as Mn, Cu, Cr, Fe, and Co oxides [7–9], become appealing due to lower cost and relative abundant resources. Amongst these catalysts, spinel-type oxides have attracted much attention for many years [1,10,11].

Among the spinel-type-oxides catalysts, Cr_2CoO_4 was found to be very active for the oxidation of hydrocarbons [10,11], as well as for catalytic removal of NO_x [12] and diesel soot [13]. As we know, doping of metal-oxide can result in a material which has significantly different properties than the original. The above has been exploited in several investigations so as to synthesize better combustion catalysts [7,14–17]. On the other hand, cerium is a well-known additive of exhaust catalysts, in view of its oxygen storage capacity, enabling the application of such catalysts over a broad range of air-to-fuel ratios, and enhancing the activity [14]. In addition, it has been reported that combination of CeO_2 with other metal oxides affects the oxygen mobility, which would play an important role in the catalytic combustion of methane [1,18]. Therefore, cerium was chosen as the dopant in the present investigation.

In this study, cerium modified cobalt chromite catalysts with different cerium content were prepared by co-precipitation method and the catalytic activities were evaluated towards methane combustion. The bulk structure was determined by Raman and XRD and the phase segregation was studied by SEM. The reducibility was studied by CH_4 TPR-MS. The oxygen desorption behavior was studied by O_2-TPD. The chemical states and surface composition

* Corresponding author at: Department of Environmental Science and Engineering, Tsinghua University, Beijing, 100084, China. Tel.: +86 10 62771093; fax: +86 10 62771093.
E-mail address: lijunhua@tsinghua.edu.cn (J. Li).

0920-5861/$ – see front matter © 2011 Elsevier B.V. All rights reserved.
doi:10.1016/j.cattod.2011.03.061

has been analyzed using XPS. In particular, the objective is to understand the promotional effect of cerium on cobalt chromite catalysts.

2. Experimental

2.1. Catalyst preparation

For cerium doped cobalt chromite catalysts, the chromium in $CoCr_2O_4$ was substituted by cerium with different substitution degree (molar ratio: 2%, 5%, 10%, 20%, 50% and 100%). The catalysts were prepared by co-precipitation method following a reference procedure [19]. Typically, a diluted aqueous ammonia (10 vol.%) solution was added to a mixed aqueous solution of chromium nitrate, cobalt nitrate and cerium nitrate drop by drop with continuous stirring at room temperature until the pH value was 9.30. The precipitates were filtered, washed several times and dried in an air oven. Finally, the dried materials were calcined at 700 °C for 4 h. The available powders were ready for the methane oxidation activity measurements after being crushed and sieved.

2.2. Catalyst characterization

The X-ray diffraction (XRD) measurements were carried out with a Rigaku D/max-2500 X-ray diffractometer using Ni filtered Cu Kα radiation. The applied current and voltage were 200 mA and 45 kV, respectively. During the analysis, the samples were scanned from 10 to 90° at a speed of 6°/min.

Raman spectra (RS) of the samples were recorded on a Renishaw RM 2000 instrument. A 633 nm He/Ne laser source at a power of 4.7 mW was used at a scanning range of 100–1200 nm.

Brunauer–Emmett–Teller (BET) surface areas and pore parameters of the samples were measured by nitrogen physisorption at liquid nitrogen temperature (77 K) on a Micromeritics ASAP 2010 micropore size analyzer. The pore size distribution was calculated from the desorption branch of the N_2 adsorption isotherm using the Barrett–Joyner–Halenda (BJH) method.

Field-emission scanning electron microscopy (SEM) was obtained by using a JEOL JSM-6700F instrument operating at a beam energy of 3.0 kV.

X-ray photoelectron spectroscopy (XPS) data were obtained with a PHI-5300/ESCA electron spectrometer with Mg and Al radiation at a pressure lower than 10^{-7} Pa. The binding energies were referenced to the C 1 s line at 284.8 eV from adventitious carbon.

Temperature programmed reduction of methane (CH_4 TPR-MS) was carried out in a quartz flow microreactor. The catalyst (100 mg), held in the quartz tube, was degassed with He (30 mL/min) at 600 °C for 1 h, and then the temperature was allowed to decrease to room temperature. The TPR tests were performed with a 20 mL/min mixture of CH_4/He (5% CH_4), at a rate of 10 °C/min from room temperature to 1000 °C maintaining finally this temperature for 100 min under the reactant mixture. Gases evolving from the reactor were analyzed with a Pfeiffer Omnistar quadrupolar mass spectrometer.

Temperature-programmed desorption of oxygen (O_2-TPD) were studied in the same system. 100 mg of the catalyst was loaded in a quartz reactor and prior the measurement, the sample was heated in a 5% O_2/He flow (30 mL/min) at 600 °C and remained in this temperature for 1 h. After cooling in O_2 to room temperature, the flowing gas was then switched to helium (20 mL/min) to eliminate the physically adsorbed oxygen. Temperature was then raised at a rate of 10 °C/min from room temperature to 1000 °C, under same helium flow. Oxygen in the reactor outlet was detected by using a quadrupolar mass spectrometer; A TCD was used for the quantification of the oxygen. The amount of O_2 desorbed from the catalysts was quantified by calibrating the peak area against that of a standard O_2 pulse (50.0 μL).

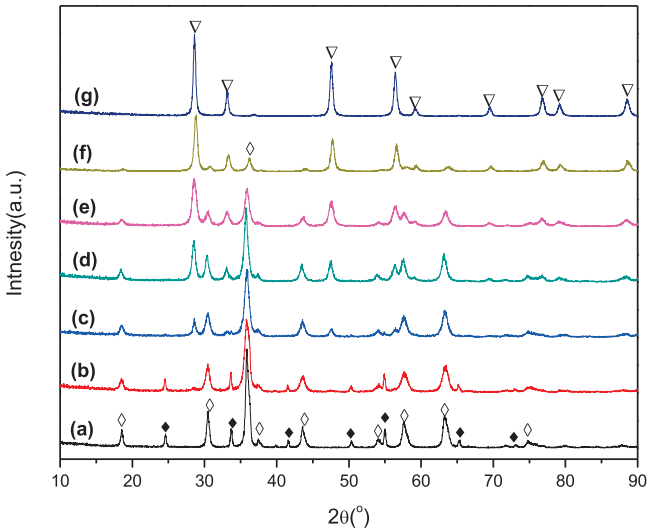

Fig. 1. XRD patterns of Ce doped Co–Cr oxides catalysts: (a) Co–Cr, (b) 2% Ce, (c) 5% Ce, (d) 10% Ce, (e) 20% Ce, (f) 50% Ce, (g) Co–Ce. Crystalline phase detected: (◊) $CoCr_2O_4$, (▽) CeO_2, (♦) Cr_2O_3.

2.3. Catalytic activity measurement

The methane combustion activities were tested in a fixed-bed quartz reactor (i.d. 8 mm) containing 250 mg catalyst. Operating conditions were as follows: 2000 ppm CH_4, 10 vol.% O_2, and N_2 as the balance gas, with a total flow rate of 150 mL/min, corresponding to a GHSV about 36,000 mL h^{-1} g^{-1}. The range of test temperature was 250 °C to 600 °C. The concentration of CH_4 in inlet and outlet gases was measured by an on-line gas chromatograph (Agilent 7890A) equipped with FID and TCD detectors. The activities were evaluated in terms of CH_4 conversion defined as $(c_{in} - c_{out})/c_{in} \times 100\%$, c_{in} and c_{out} being methane concentration corresponding to the inlet and outlet, respectively. Activity data were collected at every measurement points after stabilizing for 30 min.

3. Results and discussion

3.1. Catalyst characterization

3.1.1. The structure and morphology properties

The XRD patterns of the Co–Cr oxides and Ce modified Co–Cr oxides samples are shown in Fig. 1. The Co–Cr oxides sample was in a combined phases of cubic spinel-type $CoCr_2O_4$ (JCPDS 22-1084) and rhombic Cr_2O_3 (JCPDS 6-0504). With the doping of cerium, the intensity of chromic oxide decreased. For higher degree of cerium substitution ($x \geq 10\%$), diffraction lines corresponding to cubic CeO_2 (JCPDS 43-1002) were observed.

The Raman spectra of Ce doped cobalt chromite catalysts are compiled in Fig. 2. As shown in Fig. 2, the $CoCr_2O_4$ (sample a) spectrum shows bands at 190, 301, 342, 512, ~540, ~560, ~600, and 671 cm^{-1}. The bands at 301, 342, ~540 and ~600 cm^{-1} correspond to the vibration bands of Cr_2O_3 [20,21], and the other bands at 190, 445, 512, ~560 and 671 cm^{-1} correspond to cobalt chromite [22]. Compared to the Raman spectrum of $CoCr_2O_4$, the Raman spectra of the cerium doped samples changed a lot. For Raman spectrum of sample (b), the intensity of Raman band at ~540 cm^{-1} decreased but the intensity of band at 512 cm^{-1} increased evidently compared with the spectrum of sample (a). For sample (c) and (d), the Raman band at 512 cm^{-1} prevailed, and the weak band at 461 cm^{-1} appeared at the same time, which is characteristic band of CeO_2 [23,24]. For sample (e) and (f), the Raman band attributed to

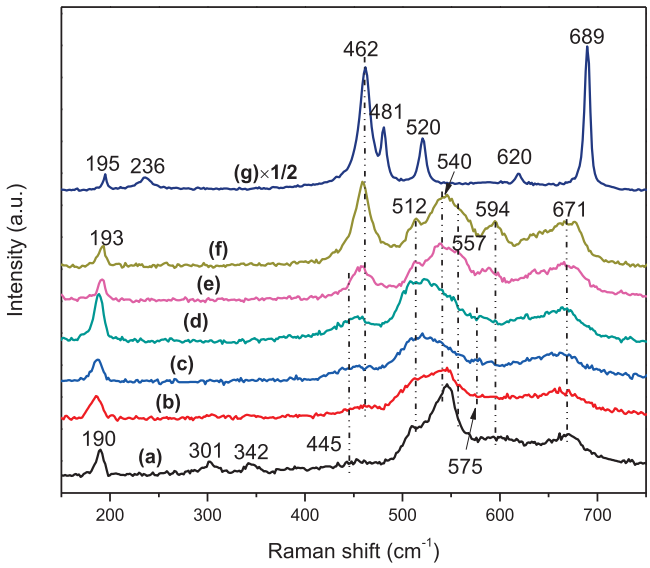

Fig. 2. Raman spectra of Ce doped Co–Cr oxides catalysts: (a) Co–Cr, (b) 2% Ce, (c) 5% Ce, (d) 10% Ce, (e) 20% Ce, (f) 50% Ce, (g) Co–Ce.

the chromium oxygen stretching vibration became dominated. The variation observed in Raman spectra might suggest that the deformation of spinel structure might occur in the process of cerium substitution. It has been reported that deformation favors oxygen mobility, affecting the redox behavior of the material [15]. Furthermore, the Raman spectrum of sample (g) shows the typical spectra of Co_3O_4 and CeO_2. The Raman bands pertaining to the Co_3O_4 appear at 195, 481, 520, 620, and 689 cm^{-1}, whereas ceria exhibits peaks at 236, and 462 cm^{-1}, which are in agreement with the literatures [23,25,26]. In addition, it's worthy to note that Raman band at 461 cm^{-1} were observed for all cerium-containing samples but shifted to higher-wavenumber positions with increasing cerium substitution degree. The narrowing and the blue-shift of the Raman bands indicate that the size of ceria particles increased with the increment of cerium content.

The values of BET surface area and pore parameters are presented in Table 1. Results indicate that BET surface areas and pore volumes increased first then decreased with the increment of Ce content. 5% Ce modified catalysts had the largest surface area and pore volume, which would benefit the catalytic performance towards methane oxidation. Significantly the surface area and pore volumes were rather small for 50% Ce and Co–Ce catalysts. This may be caused by agglomeration and sintering of CeO_2 particles (as detected by SEM, Fig. 3), which is consistent with the Raman results.

Table 1
BET surface area and pore parameters of $CoCr_2O_4$ and cerium modified cobalt chromite catalysts.

Samples	Surface area (m^2/g)	Pore volume (cm^3/g)	BJH pore diameter (nm)
Co–Cr	30.2	0.251	23.5
2% Ce	40.4	0.292	23.4
5% Ce	42.5	0.337	15.7
10% Ce	39.4	0.227	19.1
20% Ce	37.9	0.187	19.3
50% Ce	22.1	0.114	18.4
Co–Ce	13.7	0.035	3.8

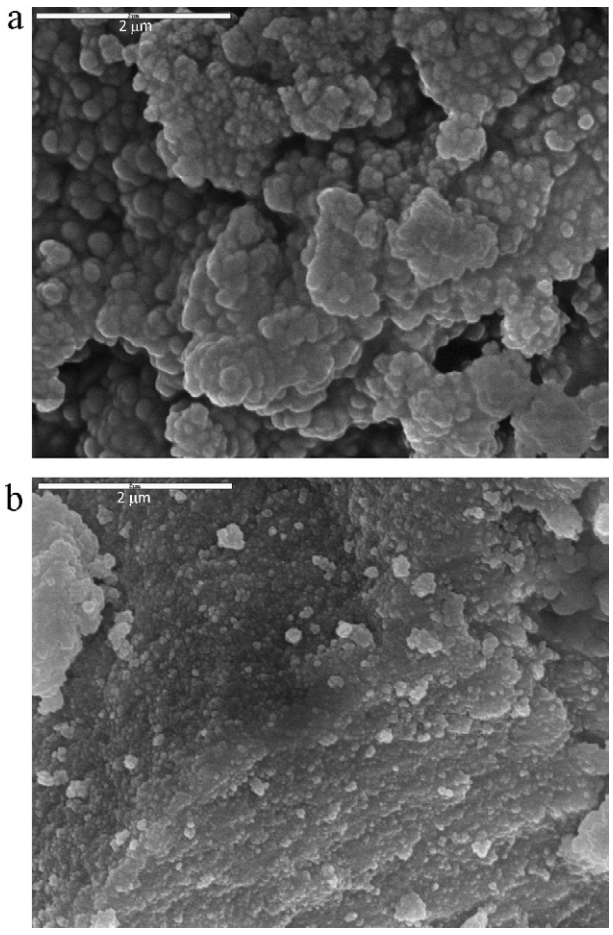

Fig. 3. SEM micrographs of (a) 5% Ce modified sample and (b) Co–Ce oxides sample.

3.1.2. CH_4 TPR-MS and O_2-TPD results

The CH_4 activation over $CoCr_2O_4$ and Ce modified catalysts was investigated via TPR-MS. The evolution of CO_2 and CO during CH_4 TPR-MS is shown in Fig. 4, and the evolution of all gases (including CO, CO_2, CH_4, H_2O and H_2) during CH_4TPR-MS tests over 5% Ce modified catalyst is also displayed in Fig. 5. For 5% Ce modified catalyst, the initial temperature of CH_4 activation was nearly the same with that of $CoCr_2O_4$, but the amount of CH_4 that is activated increased significantly. For 20% and 50% Ce modified catalysts, the activation temperature shift to higher temperatures. A similar phenomenon can be observed in the activation of CH_4 to CO during CH_4 TPR-MS (Fig. 4(B)). The 5% Ce modified catalyst had the lowest initial temperature of CH_4 activation to CO and the largest amount of CH_4 activated. Therefore, the CH_4 activation follows the order 5% Ce > Co–Cr > 20% Ce > 50% Ce. This happens because the presence of Ce deformed the structure (as stated above), and then a large number of defects might be formed during this process, resulting in numerous sites with unsaturated coordination. Since CH_4 can be more easily adsorbed on the unsaturated sites with numerous defects than on a crystal with fewer defects, its activation is facilitated by the former catalyst. Consequently the deformations caused by Ce substitution favor CH_4 activation and then enhance the reducibility of the catalysts.

A complete analysis of all the gases evolving during CH_4 TPR-MS experiments gives important hints on the processes taking place in the course of the test. As shown in Fig. 5, the process of total methane oxidation ($CH_4 + 4O_{solid} \rightarrow CO_2 + 2H_2O$) prevails at lower temperature, followed by partial oxidation processes ($CH_4 + O_{solid} \rightarrow CO + 2H_2$, $CH_4 + 2O_{solid} \rightarrow CO + 2H_2O$), while

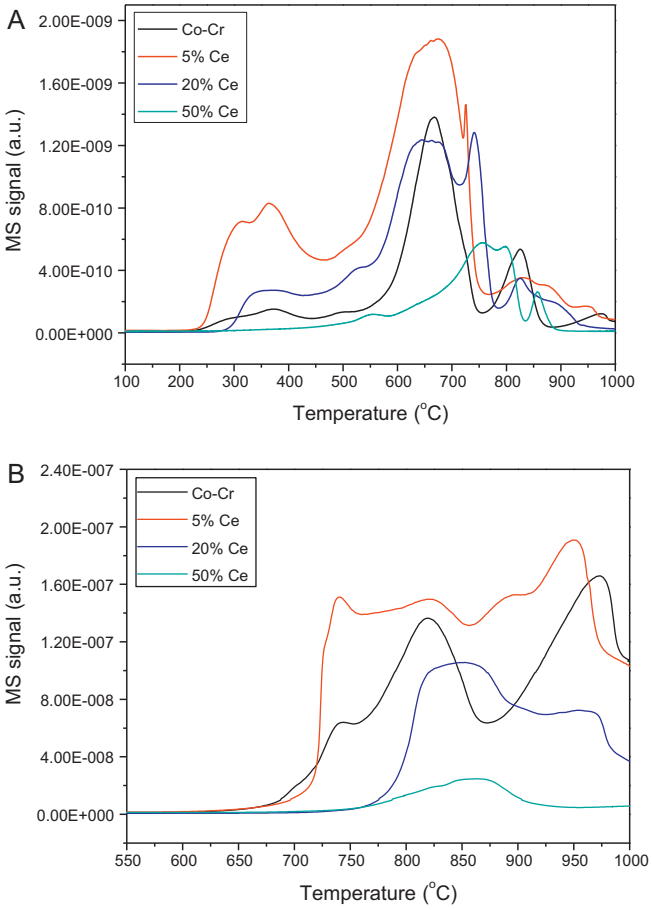

Fig. 4. Evolution of (A) $m/e = 44$ (CO_2) and (B) $m/e = 28$ (CO) signal during CH_4 TPR-MS tests.

probably methane cracking and generation of carbon deposits ($CH_4 \rightarrow C + 2H_2$) occur at high temperatures, which were in accord with the literatures [27–29].

Fig. 6 shows the results obtained during O_2-TPD tests. As widely reported in literatures [30–32], perovskite can desorb two different types of oxygen species as the temperature increased: low temperature specie, named α, desorbed when temperature is lower than 600 °C, and a high temperature one, named β, desorbed above about 600 °C. The α-oxygen can be attributed to desorption of the oxygen adsorbed on the surface, and the β-oxygen depends on the

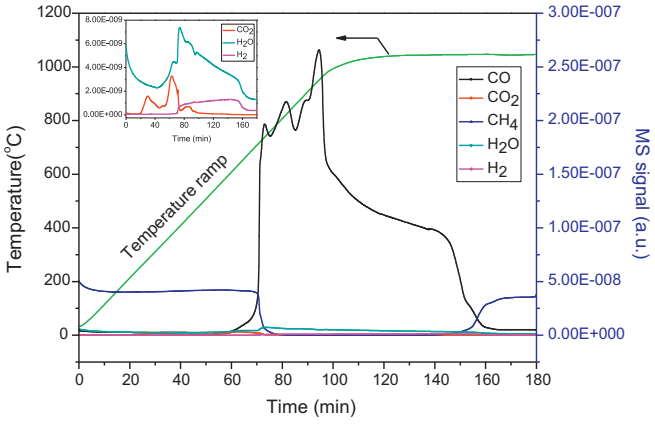

Fig. 5. Evolution of the indicated gases (including $m/e = 2$ (H_2), 15 (CH_4), 18 (H_2O), 28 (CO) and 44 (CO_2) MS signals) during the CH4TPR-MS test over 5% Ce sample (inset: evolution of CO_2, H_2O and H_2 during the CH_4 TPR-MS test).

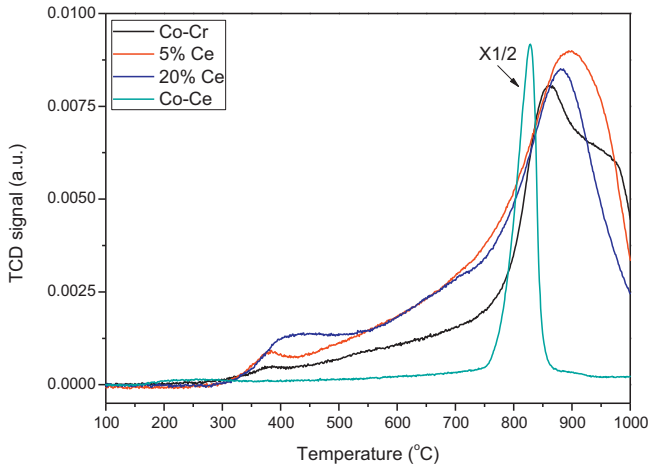

Fig. 6. O_2-TPD profiles of the indicated catalysts.

partial reduction of metal ions to a lower oxidation state. The same behavior was observed for spinels [11,13]. The results of O_2-TPD are presented in Table 2. Substitution of chromium with cerium gave rise to an increase of the amount of released oxygen, especially the α-oxygen. The 5% Ce modified catalyst got the largest amount of oxygen desorbed and also the largest β-type oxygen. It may indicate that the 5% Ce modified catalyst has better reducibility and oxygen mobility, which would play a major role in methane oxidation [33]. Furthermore, the oxygen desorption behavior of the Co–Ce catalyst was different from these of other catalysts. The α-oxygen was not observed, and a sharp β-peak appeared in the temperature range between 750 °C and 850 °C. The β-peak may be attributed to partial reduction of CeO_2 to Ce_2O_3 ($4CeO_2 \rightarrow 2Ce_2O_3 + O_2$). Accordingly, the promotional effect of Ce to β-oxygen may be due to the decomposing of ceria at high temperature.

3.1.3. Evaluation of XPS characterization

To obtain detailed information on the surface composition and local atomic environments of $CoCr_2O_4$ and Ce modified Co–Cr oxides samples, XPS spectra of $CoCr_2O_4$, 5% Ce, 20% Ce, and 50% Ce modified catalysts were carried out. The O 1s, Co 2p, Cr 2p, and Ce 3d XPS spectra are displayed in Fig. 7(A)–(D). The binding energies for the corresponding main lines of O 1s, Co 2p, Cr 2p and Ce 3d spectra and surface atomic ratios for the samples are compiled in Table 3.

As shown in Fig. 7(A), the intense main oxygen peaks have shoulders at higher binding energies, which can be resolved into two components with peaks around 531.5 and 530.1 eV, respectively, as reported in literatures [1,2,34]. The two peaks of O 1s are distinguished as O_I and O_{II}, while O_I has a binding energy about 1.4 eV higher than that of O_{II}. The O_I peaks can be associated with adsorption of oxygen species at the surface [1,34,35], while the low binding energy of O_{II} could be ascribed to lattice oxygen [2,35]. Area ratio of O_I/O_{II} could be a yardstick to measure the proportion of the two different oxygen species, thus higher area ratio indicates larger amount of vacant oxygen [1]. It can be seen from the Table 3 that 5%

Table 2
Results of O_2-TPD tests on the indicated catalysts.

Catalyst	Onset temperature	Total O_2 (mmol/g)	α-O_2 (mmol/g)	β-O_2 (mmol/g)
Co–Cr	211	2.44	0.23	2.21
5% Ce	234	3.20	0.44	2.75
20% Ce	287	2.76	0.58	2.18
Co–Ce	680	1.02	–	1.02

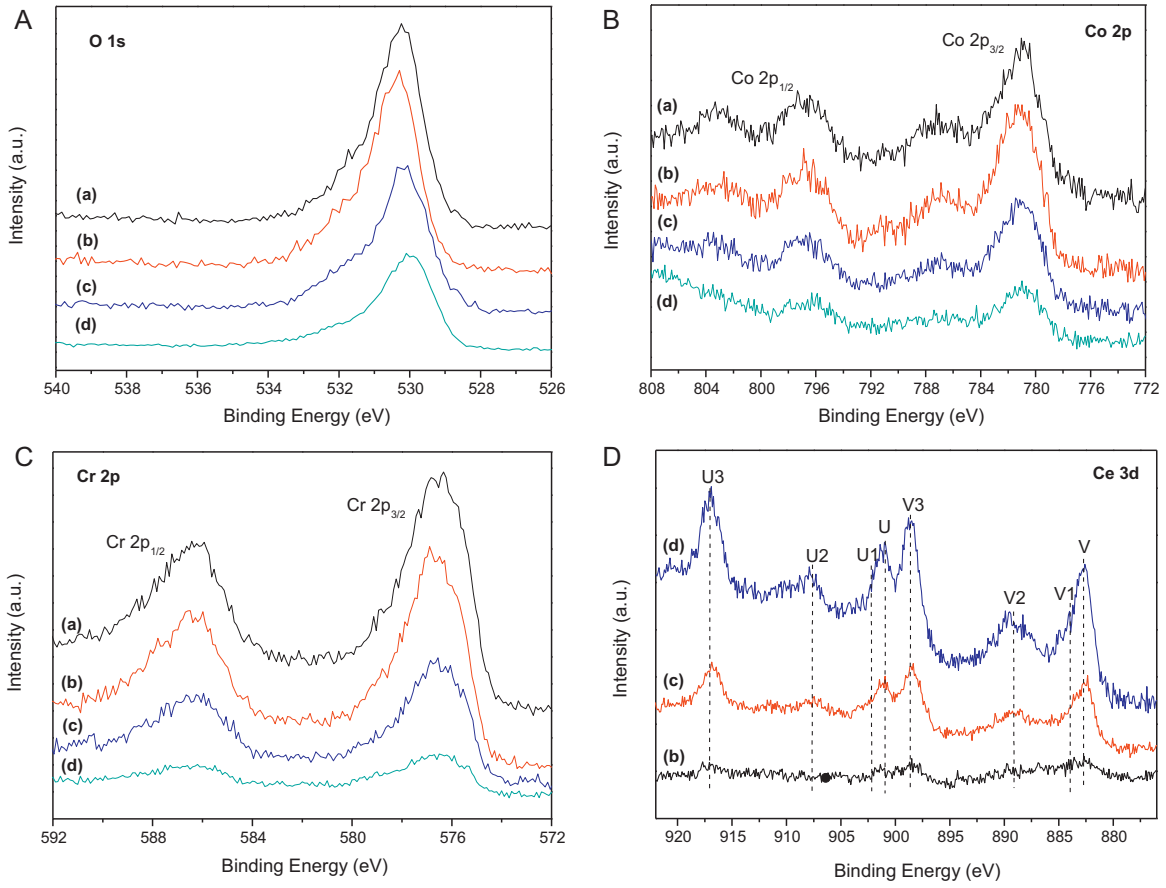

Fig. 7. XPS of O 1s level (A), Co 2p level (B), Cr 2p level (C) and Ce 3d level (D) for (a) CoCr2O4, (b) 5% Ce, (c) 20% Ce, (d) 50% Ce modified catalysts.

Ce modified catalyst had comparatively higher amount of surface oxygen than others, and the largest vacant oxygen.

In Fig. 7(B), the multiplex spectra of cobalt on four samples are shown. The spectra were fitted with the Co^{2+} and Co^{3+} components, characterized by the binding energy at about 781.7 ± 0.1 eV and 780.3 ± 0.4 eV, as reported in literatures [12,36,37]. The presence of the satellite peaks at about 6 eV from the high energy component is a further evidence for Co^{2+} species [38,39]. The relative percentage of the two cobalt species was obtained by the intensity of the Co $2p_{3/2}$ components in terms of Co^{2+} and Co^{3+}. The binding energy of Co $2p_{3/2}$ and $Co^{3+}/(Co^{3+}+Co^{2+})$ atomic ratio are summarized in Table 3. Interestingly, the atomic ratio of Co^{3+} decreased first and then increased as the content of cerium increased.

The Cr $2p_{3/2}$ spectra (Fig. 7(C)) show a clear asymmetry and are resolved into two peaks with maxima at 576.3 and 578.2 eV. The peaks were assigned to Cr^{3+} and Cr^{6+} [10,12,40], respectively. The binding energies of Cr $2p_{3/2}$ spectra and surface atomic ratios of Cr^{6+} are summarized in Table 3. The relative percentage of Cr^{6+} was estimated to be 0.33 for $CoCr_2O_4$, and for 5% Ce modified catalyst, the relative percentage of Cr^{6+} was 0.31, which was slightly lower than that of $CoCr_2O_4$. However, the percentage of Cr^{6+} for 20% and 50% modified catalyst was higher than that for $CoCr_2O_4$.

In Fig. 7(D), the Ce 3d spectra of 5%, 20% and 50% Ce modified catalysts are shown. The curves were fitted with eight peaks corresponding to four pairs of spin–orbit doublets. The bands labeled U1 and V1 represent the $3d^{10}4f^1$ initial electronic state corresponding to Ce^{3+}, while the peaks labeled U, U2, U3, V, V2 and V3 represent the $3d^{10}4f^0$ state of Ce^{4+} ions [38,41,42]. The relative percentage of the two cerium species was obtained by the intensity of the Ce $3d_{5/2}$ components relative to Ce^{4+} (V, V2, V3) and to Ce^{3+} (V1).

Table 3
XPS data of $CoCr_2O_4$ and Ce modified cobalt chromite samples.

Sample	BE (eV)				Atomic ratio				
	O 1s	Co $2p_{3/2}$	Cr $2p_{3/2}$	Ce $3d_{5/2}$	O_I/O_{II}	Co^{3+}/Co_{tot} [a]	Cr^{6+}/Cr_{tot} [b]	Ce^{3+}/Ce_{tot} [c]	Ce/Co
Co–Cr	531.6	780.7	576.3	–	0.46	0.21	0.33		
	530.2	781.7	578.0	–					
5% Ce	531.3	780.1	576.5	–	1.03	0.13	0.31		0.09
	530.3	781.6	578.4	–					
20% Ce	531.8	780.4	576.4	882.6	0.40	0.41	0.44	0.20	0.42
	530.1	781.8	578.3	885.0					
50% Ce	531.3	779.9	576.3	882.7	0.66	0.65	0.57	0.16	1.93
	530.0	–	578.4	884.5					

[a] $Co^{3+}/Co_{tot} = Co^{3+}/(Co^{3+}+Co^{2+})$.
[b] $Cr^{6+}/Cr_{tot} = Cr^{6+}/(Cr^{3+}+Cr^{6+})$.
[c] $Ce^{3+}/Ce_{tot} = Ce^{3+}/(Ce^{3+}+Ce^{4+})$.

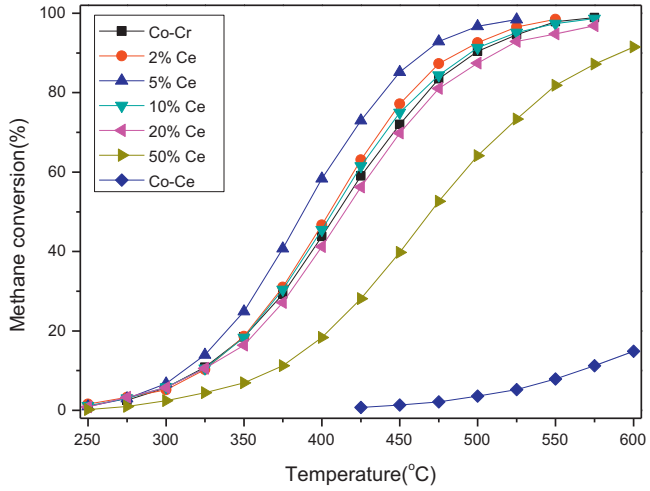

Fig. 8. Temperature dependence of methane conversion over different amount of cerium doped Co–Cr oxides. Reaction condition: 2000 ppm CH_4, 10 vol.% O_2, and N_2 as the balance gas, with a total flow rate of 150 mL/min, corresponding to a GHSV about 36,000 mL h^{-1} g^{-1}.

In Table 3, the atomic ratios of $Ce^{3+}/(Ce^{3+}+Ce^{4+})$ and Ce/Co are reported. Although it is well documented that ceria can be partial reduced during XPS characterization [38,41], we cannot exclude the possibility that Ce^{3+} exists at the surface. By comparing the Ce/Co atomic ratio of 50% Ce sample with that of 5% Ce and 20% Ce samples, cerium enrichment of the surface was observed upon samples with higher substitution degree.

It is interesting to note that the relative percentage of Co^{3+} and Cr^{6+} for 5% Ce modified catalyst was lower than that of $CoCr_2O_4$ catalyst. This is possibly because charge compensating occurs so as to maintain charge balance when a foreign cation with different oxidation state was introduced into the system. The normal oxidation state of cerium is +4, which is higher than normal valence of cobalt and chromium in spinel lattice, so electroneutrality can be achieved either by formation of oxygen vacancies or by lowering the oxidation state of cobalt and/or chromium. Therefore, the percentage of Co^{3+} and Cr^{6+} of 5% Ce modified catalyst was lower than that of $CoCr_2O_4$.

3.2. Catalytic activity for methane combustion

The catalytic activities were evaluated towards methane combustion, and the results are shown in Fig. 8. The catalytic tests indicate that, in the temperature range investigated, all the catalysts show 100% selectivity towards CO_2, and no CO was observed during the reaction. As shown in Fig. 8, substitution of Cr with appropriate amount of Ce promoted the catalytic activity of the catalysts. However, large amount of Ce substitution reduced the activity, especially for samples with substitution degree higher than 20%. The 2%, 5% and 10% Ce modified catalysts all had better methane conversion than the undoped catalyst. The highest methane conversion was obtained over 5% Ce modified catalysts, and the T_{90} (the temperature needed to reach 90% methane conversion) was as low as 465 °C. The lowest methane conversion was found over Co–Ce catalyst. In summary, if T_{90} was set as standard of activity, the descending order of activity for all the observed catalysts was as follows: 5% Ce > 2% Ce > 10% Ce > Co–Cr > 20% Ce > 50% Ce > Co–Ce.

It is interesting to note that the sequence of catalytic activity consistent with the sequence of CH_4 activation obtained from the CH_4 TPR-MS tests and the temperature at which CH_4 oxidation began was very close to the initial temperature of CH_4 activation (Figs. 4 and 8). So it is plausible to suggest CH_4 adsorption and even activation on the catalyst may be a necessary and rate-limiting step in methane oxidation reaction, as reported in the literatures [43,44]. The main difference between CH_4 TPR-MS investigations and activity tests lies on the availability of oxygen resources during the adsorption and activation of CH_4. For CH_4 TPR-MS tests (absence of added oxidant), the oxygen resources were lattice oxygen and adsorbed active oxygen at the surface at low temperature, but at higher temperature, the oxygen may origin from the bulk oxygen, whose rate is affected by the low diffusion of the oxygen towards the surface. However, during the activity tests, methane adsorption is required, but the activation products of methane can be rapidly and completely oxidized into carbon dioxide and water. Simultaneously, the lattice oxygen consumed at the surface would be quickly replenished and reach equilibrium with gas phase oxygen. So the temperature at which the optimum activity was attained was lower than that of CH_4 TPR-MS tests in the absence of oxygen.

The T_{90} of Ce modified catalysts decreased first and then increased as the Ce content increased with the lowest result for 5% Ce modified catalyst. Interestingly, the change trends of the relatively percentage of Co^{3+} and Cr^{6+} at the surface (Table 3) seem to be the same with that of T_{90}. It may indicate that charge compensating occurs during the process of Ce substitution, and the redistribution of metal ions at the surface would influence the catalytic activity towards methane oxidation. Furthermore, from the results of O_2-TPD and XPS, one can observe that the 5% Ce modified catalyst has relatively larger concentration of oxygen vacancies and more adsorbed oxygen, which may favor the adsorption, activation and then oxidation of CH_4.

For higher substitution degree, ceria enriched and sintered at the surface (Figs. 1–3), resulting in lower surface area, thus leading to the decline of the catalytic activity.

4. Conclusions

Substitution of chromium in $CoCr_2O_4$ by cerium with appropriate amount can enhance the catalytic activity of cobalt chromite in methane combustion. The best result has been attained with 5% cerium modified catalyst, and the catalytic activity reached 90% of methane conversion at 465 °C. This improvement is related to structure deformation caused in the process of substitution; consequently, it would increase crystal defects and oxygen vacancy concentration, which facilitate oxygen mobility and thus increase the catalytic performance of cerium modified cobalt chromite catalysts.

Acknowledgments

Financial support by the national High-Tech Research and Development (863) Program of China (Grant No. 2009AA064806) and special fund of State Key Joint Laboratory of Environment Simulation and Pollution Control (10Z01ESPCT) is gratefully acknowledged.

References

[1] J. Li, X. Liang, S. Xu, J. Hao, Appl. Catal. B 90 (2009) 307.
[2] J. Li, H. Fu, L. Fu, J. Hao, Environ. Sci. Technol. 40 (2006) 6455.
[3] P. Gelin, M. Primet, Appl. Catal. B 39 (2002) 1.
[4] R.J. Farrauto, M.C. Hobson, T. Kennelly, E.M. Waterman, Appl. Catal. A 81 (1992) 227.
[5] R. Ramirez-Lopez, I. Elizalde-Martinez, L. Balderas-Tapia, Catal. Today 150 (2010) 358.
[6] S.K. Matam, M.H. Aguirre, A. Weidenkaff, D. Ferri, J. Phys. Chem. C 114 (2010) 9439.
[7] T.V. Choudhary, S. Banerjee, V.R. Choudhary, Appl. Catal. A 234 (2002) 1.
[8] J. Kirchnerova, D. Klvana, Catal. Lett. 67 (2000) 175.
[9] C. Lahousse, A. Bernier, P. Grange, B. Delmon, P. Papaefthimiou, T. Ioannides, X. Verykios, J. Catal. 178 (1998) 214.
[10] D.C. Kim, S.-K. Ihm, Environ. Sci. Technol. 35 (2001) 222.

[11] D. Fino, N. Russo, G. Saracco, V. Specchia, Catal. Today 117 (2006) 559.
[12] J. Sloczynski, J. Janas, T. Machej, J. Rynkowski, J. Stoch, Appl. Catal. B 24 (2000) 45.
[13] D. Fino, N. Russo, G. Saracco, V. Specchia, J. Catal. 242 (2006) 38.
[14] Y. Zhang-Steenwinkel, J. Beckers, A. Bliek, Appl. Catal. A 235 (2002) 79.
[15] A. Bueno-Lóez, K. Krishna, M. Makkee, J.A. Moulijn, J. Catal. 230 (2005) 237.
[16] B. Bialobok, J. Trawczynski, W. Mista, M. Zawadzki, Appl. Catal. B 72 (2007) 395.
[17] J. Deng, L. Zhang, H. Dai, H. He, C.T. Au, Appl. Catal. B 89 (2009) 87.
[18] L. Xue, C. Zhang, H. He, Y. Teraoka, Appl. Catal. B 75 (2007) 167.
[19] G.J. Hutchings, R.G. Copperthwaitet, F.M. Gottschalk, R. Hunter, J. Mellor, S.W. Orchard, T. Sangiorgio, J. Catal. 137 (1992) 408.
[20] H.Y. Chen, F.-H. Lu, Thin Solid Films 515 (2006) 2179.
[21] M. Cherian, M.S. Rao, A.M. Hirt, I.E. Wachs, G. Deo, J. Catal. 211 (2002) 482.
[22] B.J. Reddy, R.L. Frost, Spectrochim. Acta A 61 (2005) 1721.
[23] B.M. Reddy, A. Khan, P. Lakshmanan, M. Aouine, S. Loridant, J.-C. Volta, J. Phys. Chem. B 109 (2005) 3355.
[24] J. Fang, X. Bi, D. Si, Z. Jiang, W. Huang, Appl. Surf. Sci. 253 (2007) 8952.
[25] V.G. Hadjiev, et al., J. Phys. C: Solid State Phys. 21 (1988) L199.
[26] X.X. Gao, C.J. Huang, N.W. Zhang, J.H. Li, W.Z. Weng, H.L. Wan, Catal. Today 131 (2008) 211.
[27] A. Hornes, D. Gamarra, G. Munuera, A. Fuerte, R.X. Valenzuela, M.J. Escudero, L. Daza, J.C. Conesa, P. Bera, A. Martinez-Arias, J. Power Sources 192 (2009) 70.
[28] A. Hornes, D. Gamarra, G. Munuera, J.C. Conesa, A. Martinez-Arias, J. Power Sources 169 (2007) 9.
[29] Y.H. Hu, E. Ruckenstein, Langmuir 13 (1997) 2055.
[30] B. Levasseur, S. Kaliaguine, Appl. Catal. B 88 (2009) 305.
[31] L. Marchetti, L. Forni, Appl. Catal. B 15 (1998) 179.
[32] L.M.T. Simplicio, S.T. Brandao, E.A. Sales, L. Lietti, F. Bozon-Verduraz, Appl. Catal. B 63 (2006) 9.
[33] L. Forni, I. Rossetti, Appl. Catal. B 38 (2002) 29.
[34] A. La Rosa-Toro, R. Berenguer, C. Quijada, F. Montilla, E. Morallon, J.L. Vazquez, J. Phys. Chem. B 110 (2006) 24021.
[35] J. Zhu, Q. Gao, Micropor. Mesopor. Mater. 124 (2009) 144.
[36] W. Wei, W. Chen, D.G. Ivey, Chem. Mater. 20 (2008) 1941.
[37] Z. Zsoldos, L. Guczi, J. Phys. Chem. 96 (1992) 9393.
[38] L.F. Liotta, G. Di Carlo, G. Pantaleo, A.M. Venezia, G. Deganello, Appl. Catal. B 66 (2006) 217.
[39] D. Pietrogiacomi, S. Tuti, M.C. Campa, V. Indovina, Appl. Catal. B 28 (2000) 43.
[40] J.R. Mellor, R.G. Copperthwaite, N.J. Coville, Appl. Catal. A 164 (1997) 69.
[41] L. Qiu, F. Liu, L. Zhao, Y. Ma, J. Yao, Appl. Surf. Sci. 252 (2006) 4931.
[42] F. Larachi, J. Pierre, A. Adnot, A. Bernis, Appl. Surf. Sci. 195 (2002) 236.
[43] W. Liu, M. Flytzanistephanopoulos, J. Catal. 153 (1995) 317.
[44] W. Liu, M. Flytzanistephanopoulos, J. Catal. 153 (1995) 304.